Transceiver Design for MIMO ZP-OTFS-SCMA System with Physical Layer Security

Md. Najmul Hossain[1,*], SK. Tamanna Kamal[2], Jinia Rahman[3], Shaikh Enayet Ullah[2], and Tetsuya Shimamura[4]

[1] Department of Electrical, Electronic and Communication Engineering, Pabna University of Science and Technology, Pabna-6600, Bangladesh
[2] Department of Electrical and Electronic Engineering, University of Rajshahi, Rajshahi-6205, Bangladesh
[3] Department of Electrical and Electronic Engineering Khwaja Yunus Ali University, Enayetpur, Sirajgonj-6700, Bangladesh
[4] Graduate School of Science and Engineering, Saitama University, Shimo-Okubo 255, Sakura-ku, Saitama 338-8570, Japan
Email: najmul_eece@pust.ac.bd (M.N.H.); tamanna.eee.ru@gmail.com (SK.T.K.); jinia4944@gmail.com (J.R.); enayet_apee@ru.ac.bd (S.E.U.); shima@mail.saitama-u.ac.jp (T.S.)
*Corresponding author

***Abstract*—In this paper, we present an mmWave multiantenna configured transceiver for Sparse Code Multiple Access (SCMA) schemes implemented in an Orthogonal Time Frequency Space (OTFS) system. Our proposed system introduces a 6-D hyperchaotic mapping system-aided encryption algorithm to enhance physical layer security (PLS). Additionally, Turbo, Low-Density Parity Check (LDPC) and repeat and accumulate (RA) channel coding, modified form of Delay-Doppler (DD)-domain SCMA codeword allocation, Log-domain Message Passing Algorithm (Log-MPA)-based SCMA decoding, Cholesky Decomposition-Based ZF (CD-ZF) and Minimum Mean Square Error (MMSE) signal detection schemes are introduced for achieving improved Bit Error Rate (BER). The numerical results demonstrate the effectiveness of the proposed system in terms of PLS enhancement with low correlation coefficients (15.54%, 16.00%, 26.11%, 22.39%, 19.45%, and 18.68% for Users 1, 2, 3, 4, 5, and 6, respectively) on synthetically generated binary data transmission. Our system achieves a Complementary Cumulative Distribution Function (CCDF) of Peak-to-Average Power Ratio (PAPR) of 6.61 dB at its 0.1% probability level. The six users achieve a BER of 1×10^{-4} at signal-to-noise ratios (SNRs) of 6.5 dB, 15 dB, 8.5 dB, 6.5 dB, 9.5 dB, and 8.5 dB underutilization of turbo channel coding and MMSE signal detection schemes. In the case of turbo channel coding and CD-ZF signal detection schemes, the BER performance for all six users approaches zero for SNR values ranging from 0 dB to 20 dB.**

***Keywords*—Orthogonal Time Frequency Space (OTFS), Sparse Code Multiple Access (SCMA), bit error rate, channel coding, peak-to-average power ratio, physical layer security encryption, Signal-to-Noise Ratio (SNR)**

I. Introduction

With the rapid advancement of smart terminals and the emergence of envisaged applications (such as real-time and interactive services), wireless data traffic has significantly increased in commercially deployed 5G cellular networks. However, these networks are unable to keep up with the escalating technological requirements. Sixth-generation (6G) mobile networks are anticipated to cast high-tech new-spectrum and energy-efficient transmission techniques in order to face the upcoming difficulties [1]. In 4th- and 5th-generation wireless networks, Orthogonal Frequency Division Multiplexing (OFDM) has been used as a multicarrier signal waveform, and its performance degrades due to the Doppler effect in high-mobility environments [2]. The 6G mobile network will hopefully meet the crucial challenge and provide dependable communication in a variety of use cases, such as Mobile Communications on board Aircraft (MCA), Low-Earth-Orbit satellites (LEOs), self-driving autonomous cars, in-vehicle infotainment, and Unmanned Aerial Vehicles (UAVs), high-speed rail, and vehicle-to-everything (V2X) in high-mobility environments, etc. In future high-mobility use cases, a novel Two-Dimensional (2D) modulation scheme, Orthogonal Time Frequency Space (OTFS), has emerged as a key enabler. Unlike OFDM, which uses the Time-Frequency (TF) domain for information modulation, OTFS uses the delay-Doppler (DD) domain to offer advantages such as Doppler and delay resilience, reduced signaling latency, a lower Peak-to-Average Power Ratio (PAPR) and reduced complexity implementation [3, 4]. In upcoming 6G networks, Sparse Code Multiple Access (SCMA), which is one of the most promising code-domain Nonorthogonal Multiple Access (NOMA) techniques, has been emphasized as an enabling factor to support high data rates, system capacity, and spectral efficiency [5]. The SCMA technology, with superior time-frequency resource utilization capability, can provide massive connectivity and timely computing in

Manuscript received May 28, 2024; revised July 12, 2024; accepted August 30, 2024; published October 16, 2024.

Unmanned Aerial Vehicle (UAV)-assisted Mobile Edge Computing (MEC) networks [6]. However, in continuation of further development of OTFS technology with consideration of the superior time-frequency resource utilization capability of SCMA technology, a transceiver has been designed in this paper with the combination of OTFS and SCMA technology. In the proposed downlink SCMA-OTFS MIMO system, a 6-D hyperchaotic mapping system-based Physical Layer Security (PLS) encryption technique [7] has been implemented to make the exchange of information between the transmitting and receiving ends nonvulnerable to malicious attacks due to the openness of wireless communication systems.

A. Related Works

The features and performance of SCMA, OTFS, and SCMA-OTFS schemes are attracting the scientific community's attention. Several contributions have been presented in the last few years. Ge [8] *et al.* developed a customized Gaussian Approximation with an Expectation Propagation (GAEP) algorithm for multiuser detection and proposed efficient algorithm structures for centralized and decentralized detectors for multiple mobile users grouped for SCMA. Liu [6] *et al.* investigated the long-term task latency and energy consumption minimization issues in SCMA-enhanced UAV-MEC networks and proposed an algorithm that was capable of achieving convergence with more significant advantages over the other benchmark algorithms. An experimental study was performed in [9] to present a comparison among the Orthogonal Frequency Division Multiplexing (OFDM), Filter Bank Multicarrier (FBMC), and Orthogonal Time Frequency Space (OTFS) waveforms in a terahertz photonic-wireless point-to-point communication system operating at 300 GHz. A reasonably acceptable Bit Error Rate (BER) performance was achieved in the OTFS waveform. By integrating SCMA and OTFS, Deka *et al.* [10] proposed a multiuser OTFS system based on SCMA and compared its performance with OTFS-OMA, OFDM-SCMA, and OTFS-Power-Domain (PD)-NOMA techniques.

Along with the BER performance, the analysis of OTFS-SCMA with channel estimation was also reported in their work. Based on the diversity analysis, an algorithm was proposed to create an ideal code word allocation scheme. Thomas *et al.* [11] presented Orthogonal Time Sequency Multiplexing (OTSM), a variant of the OTFS-based OTSM-SCMA scheme, which achieved BER performance comparable to that of the OTSM-OMA scheme. Deng *et al.* [12] proposed a novel resource hopping mechanism for Orthogonal Time Frequency Space (OTFS) systems with delay, or Doppler partitioned Sparse Code Multiple Access (SCMA) to mitigate the effect of jamming in a controlled multiuser uplink. All these contributions show that the integrated SCMA-OTFS scheme can be a strong candidate for future-generation multiuser wireless systems. Ge *et al.* [13] developed a novel low-complexity effective customized memory Approximate Message Passing (AMP) algorithm for channel equalization and multiuser detection under consideration of a Nonorthogonal Sparse Code Multiple Access (SCMA) configuration for Multiple-input Multiple-output (MIMO) systems with Orthogonal Time Frequency Space (OTFS) modulation. In their simulation works, such a memory AMP detector was found to be robust compared to other detectors. Li and Hong [14] considered an Intelligent Reflecting Surface (IRS)-aided orthogonal time frequency space (OTFS)-based uplink Sparse Code Multiple Access (SCMA) communications system. They conducted performance analysis in terms of Pairwise Error Probability (PEP) and derived an upper bound on Word Error Probability (WEP). Their simulation results demonstrated that their proposed IRS design algorithms achieved better error performance than the known approaches.

B. Contribution and Organization

The major concern of this paper is to create a novel framework for a zero-padded secure mmWave MIMO OTFS-SCMA system. The significant contributions of the paper are outlined as follows:

- The applicability of the zero-padding scheme in the prepended and appended form to each block of an OTFS frame is proposed to reduce inter-block interference (IBI), OOB spectral power, and adjacent-channel interference (ACI).
- Sun's proposed new 6-D hyperchaotic system [7] is implemented as a cryptographic technique for physical layer security (PLS) encryption in this suggested system.
- A significant enhancement in the BER performance of the proposed system is achieved from the simulation results.
- Proper identification of the proposed system-compatible FEC channel coding scheme

The remainder of this paper is organized as follows. Section II introduces the system model of our proposed secure multiuser mmWave pre- and post-zero-padded MIMO SCMA-OTFS system, including the network description, block diagram, and signal model. Numerical results and discussions are presented in Section III. Finally, Section IV provides a summary and concluding remarks. Throughout the paper, the notations $(:)T$, $(:)H$ and $\|.\|^2$ denote the non-conjugate transpose, Hermitian transpose, and square of the Euclidian norm of the matrix operation, respectively.

II. System Model

A. Preliminaries of OTFS-SCMA System

Sparse Code Multiple Access (SCMA) is a nonorthogonal multiple access scheme that allows an increase in the number of active users inside a given time-frequency resource. In the SCMA encoding scheme, we map every $log_2(\bar{M})$ encoded bits of individual users to a K -dimensional complex codebook of size $\bar{M}\ (=4)$, where $K\ (=4)$ is the number of orthogonal frequency division multiple access subcarriers (resource elements, REs) over which $J\ (=6)$ users, usually called layers, can transmit information simultaneously. The overloading factor is defined as $\lambda = J/K = 150\%$. The sparse codebook for each of the six users can be written as:

$$CB_1 = \begin{bmatrix} 0.0000 + 0.0000i & 0.0000 + 0.0000i & 0.0000 + 0.0000i & 0.0000 + 0.0000i \\ -0.5722 + 0.8201i & 0.5912 - 0.8065i & -0.7322 - 0.6810i & 0.6974 + 0.7167i \\ 00.0000 + 0.0000i & 0.0000 + 0.0000i & 0.0000 + 0.0000i & 0.0000 + 0.0000i \\ -0.8252 - 0.5648i & 0.0555 - 0.9985i & -0.0736 + 0.9973i & 0.8310 + 0.5562i \end{bmatrix}$$

$$CB_2 = \begin{bmatrix} -0.4426 + 0.8967i & 0.3595 + 0.9332i & -0.3428 - 0.9394i & 0.4171 - 0.9089i \\ 0.0000 + 0.0000i & 0.0000 + 0.0000i & 0.0000 + 0.0000i & 0.0000 + 0.0000i \\ 0.9366 + 0.3503i & -0.9458 - 0.3247i & 0.3366 - 0.9417i & -0.3229 + 0.9464i \\ 0.0000 + 0.0000i & 0.0000 + 0.0000i & 0.0000 + 0.0000i & 0.0000 + 0.0000i \end{bmatrix}$$

$$CB_3 = \begin{bmatrix} 0.7621 - 0.6475i & -0.7065 + 0.7077i & -0.9837 + 0.1800i & 0.9728 - 0.2315i \\ 0.9777 + 0.2101i & 0.9010 - 0.4338i & -0.9051 + 0.4252i & -0.9700 - 0.2430i \\ 0.0000 + 0.0000i & 0.0000 + 0.0000i & 0.0000 + 0.0000i & 0.0000 + 0.0000i \\ 0.0000 + 0.0000i & 0.0000 + 0.0000i & 0.0000 + 0.0000i & 0.0000 + 0.0000i \end{bmatrix} \quad (1)$$

$$CB_4 = \begin{bmatrix} 0.0000 + 0.0000i & 0.0000 + 0.0000i & 0.0000 + 0.0000i & 0.0000 + 0.0000i \\ 0.0000 + 0.0000i & 0.0000 + 0.0000i & 0.0000 + 0.0000i & 0.0000 + 0.0000i \\ -0.7252 - 0.6886i & -0.0082 + 1.0000i & 0.7561 + 0.6545i & -0.0346 - 0.9994i \\ -0.5826 - 0.8127i & 0.8803 - 0.4744i & -0.8820 + 0.4712i & 0.5885 + 0.8085i \end{bmatrix}$$

$$CB_5 = \begin{bmatrix} 0.9677 + 0.2523i & -0.9707 - 0.2401i & -0.5245 - 0.8514i & 0.5474 + 0.8369i \\ 0.0000 + 0.0000i & 0.0000 + 0.0000i & 0.0000 + 0.0000i & 0.0000 + 0.0000i \\ 0.0000 + 0.0000i & 0.0000 + 0.0000i & 0.0000 + 0.0000i & 0.0000 + 0.0000i \\ -0.4567 + 0.8896i & -0.9996 + 0.0280i & 0.9999 - 0.0120i & 0.4548 - 0.8906i \end{bmatrix}$$

$$CB_6 = \begin{bmatrix} 0.0000 + 0.0000i & 0.0000 + 0.0000i & 0.0000 + 0.0000i & 0.0000 + 0.0000i \\ -0.2429 + 0.9701i & 0.4551 + 0.8905i & -0.4806 - 0.8769i & 0.2599 - 0.9656i \\ 0.7158 - 0.6983i & -0.9978 + 0.0664i & 0.9989 - 0.0464i & -0.7197 + 0.6943i \\ 0.0000 + 0.0000i & 0.0000 + 0.0000i & 0.0000 + 0.0000i & 0.0000 + 0.0000i \end{bmatrix}$$

where CB_j is a codebook for user j. The data alphabet with four symbols $\{0,\ 1,\ 2,\ 3\}$ of user j are represented by sparse codewords, $X_j^{(m)} = (X_{j,1}^{(m)}, \ldots \ldots X_{j,K}^{(m)})^T \in \mathbb{C}^{\bar{M}\times 1}$, where $m = 1, 2, 3, 4$ is the assigned column of the codebook CB_j. The codewords of all users are superimposed and exchanged over the K REs to form a SCMA codeword $\bar{X}$, which can be written as [11, 15].

$$\bar{X} = \sum_{j=1}^{J} X_j^{(m)} \quad (2)$$

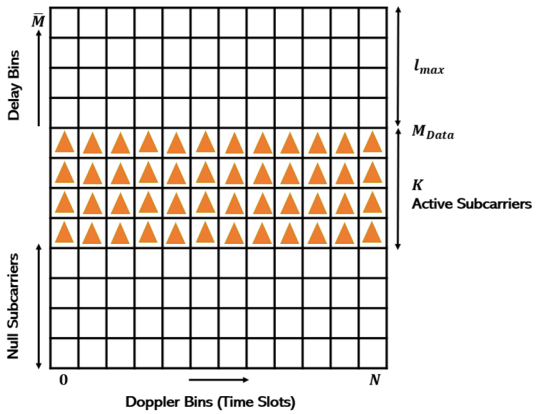

Fig. 1. SCMA codeword allocation in the DD grid, $N = 12$, $M = 12$, $lmax = 4$, $K = 4$.

Generally, the SCMA codeword $\bar{X}$ is allocated to delay-Doppler domain SCMA codeword generation, where active subcarriers are prepended with null subcarriers and the number of null subcarriers in every time slot is equal to or greater than the maximum channel delay tap, $lmax$ $(= 4)$. In our system, we consider that the active subcarriers are prepended and appended with null subcarriers and present $M \times N$ - sized SCMA codeword allocation-based DD gridded data (Fig. 1), where N is the number of Doppler bins (time slots), and M is the number of delay bins (active and null subcarriers). Such consideration could hopefully combat severe multipath channel delay spread with maximum channel delay tap and reduce interblock interference within the DD grid SCMA codebook from consecutive time slots (Doppler bin).

The DD gridded data are fed into OTFS modulation using various signal processing techniques. In the OTFS demodulation stage [16], the SCMA codewords are detected, which must be segregated or decoded to retrieve the user's binary bits. This operation can be effectively performed using an iterative factor graph-based log-message passing algorithm (log-MPA) multiuser detection algorithm, which reduces the implementation complexity as compared to MPA and the maximum posterior probability (MAP). The iterative factor graph-based Log-MPA detection algorithm is based on passing messages among concerned nodes. The nodes are the users, which are also considered the Variables Nodes (VNs); the subcarriers (or REs), which are also considered the Function Nodes (FNs); and the massages, which are the extrinsic information among nodes. This mechanism is illustrated in Fig. 2.

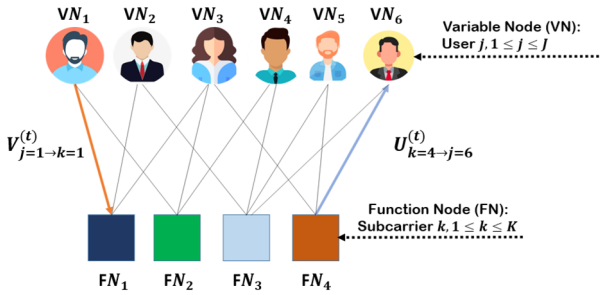

Fig. 2. Mechanism of exchange of extrinsic information among Variable Nodes (VNs) and Function Nodes (FNs).

Initially, each user expects to receive any codeword among the equally $\bar{M}$ ones:

$$V_{j\to k}^{0}(X_j^{(m)}) = \mathbb{P}(X_j^{(m)}) = \frac{1}{\bar{M}}, j = 1, \dots, J, k \in \Re(j) \quad (3)$$

In extrinsic information exchange among VNs and FNs for an assigned number of iterations, $t \le N_{iter}$. The message to be sent from FN_k, $k = 1, \dots, K$, to VN_j, $j \in u(k)$, for each codeword $X_j^{(m)} \in C_j$, $m = 1, \dots, \bar{M}$, is computed by

$$U_{k\to j}^{t}(X_j^{(m)}) = \sum_{X_i^{(m)}|i\in\Im(k)\setminus j} exp\{-\frac{1}{N_0}\|y_k - \sum_j h_{j,k}\, x_{j,k}^{(m)}\|^2\} \prod_{i\in\Im(k)\setminus j} V_{i\to k}^{t-1}(x_i^{(m)}) \quad (4)$$

where N_0 is the AWGN noise variance, $h_{j,k}$ is the channel gain of user j on subcarrier k, and y_k is the received signal on the k^{th} subcarrier.

The message to be sent from $V_{N,j}, j = 1, \dots, J$ to FN_k, $k \in \Re(j)$, for each codeword $X_j^{(m)} \in C_j$, $m = 1, \dots, \bar{M}$, is calculated as:

$$V_{j\to k}^{t}(x_j^{(m)}) = \frac{\prod_{i\in\Re(j)\setminus k} U_{i\to j}^{t-1}(x_j^{(m)})}{\sum X_j^{(l)}\in C_j \prod_{i\in\Re(j)\setminus k} U_{i\to j}^{t-1}(x_j^{(l)})} \quad (5)$$

It is essential to normalize this message to guarantee the numerical stability of such a Log-MPA technique. In estimating the received bits, the posterior probability of each codeword for each user is represented by

$$\mathbb{P}(X_j^{(m)}) = \prod_{k\in\Re(j)} U_{k\to j}^{N_{iter}}(x_j^{(m)}), m = 1, \dots \bar{M}, j = 1, \dots, J. \quad (6)$$

The Log-Likelihood Rate (LLR) for each coded bit, bi, $1 \le i \le log2(\bar{M})$, is given by

$$\begin{aligned} &LLR(b_i) \\ &= [\max_{\{X_j^{(m)}\in C_j|b_i=0\}} (log(\mathbb{P}(X_j^{(m)}))) + log(1 \\ &+ \sum_{m'\in\{1\dots M\}\setminus m} exp(-|log(\mathbb{P}(X_j^{(m)})) \\ &- log(\mathbb{P}(X_j^{(m')}))|))] \\ &- [\max_{\{X_j^{(m)}\in C_j|b_i=1\}} (log(\mathbb{P}(X_j^{(m)}))) + log(1 \\ &+ \sum_{m'\in\{1\dots M\}\setminus m} exp(-|log(\mathbb{P}(X_j^{(m)})) \\ &- log(\mathbb{P}(X_j^{(m')}))|))] \end{aligned} \quad (7)$$

Finally, the value of each LLR is used to determine the corresponding bit as follows [17]:

$$\hat{b}_i = \begin{cases} 1 \; if \; LLR(b_i) \le 0 \\ 0 \; otherwise \end{cases} \quad (8)$$

Our proposed MIMO ZP-OTFS-SCMA system is an advanced communication system, and its SCMA encoding is typically low. Due to the need for numerous iterations for convergence, computationally demanding message passing operations, and large factor graphs with multiple nodes and edges, the iterative factor graph-based Log-MAP algorithm for SCMA is thought to have high complexity; however, it achieves better decoding performance and can effectively handle the sparsity of SCMA. Implementing SCMA and OTFS modulation schemes makes our system energy-efficient by supporting multiple users with lower energy consumption per user and mitigating the impact of Doppler shifts and channel distortions in high-mobility and multipath scenarios. In terms of user scalability, the SCMA-OTFS systems can support many users due to SCMA's sparse codebook design and OTFS's efficient time-frequency resource allocation [18–20].

B. Scenario Descriptions

A scenario of mmWave downlink signal transmission is presented in Fig. 3 for a secure MIMO ZP-OTFS- SCMA system. In such terrestrial cellular networking, one ground base station and six ground users riding on moving vehicles are considered, each of which is equipped with two transmit/receive antennas. In the scenario of a high-mobility environment, some special type of delay-Doppler communication strategy is adopted to meet the limitations of multicarrier techniques over channels with high mobility.

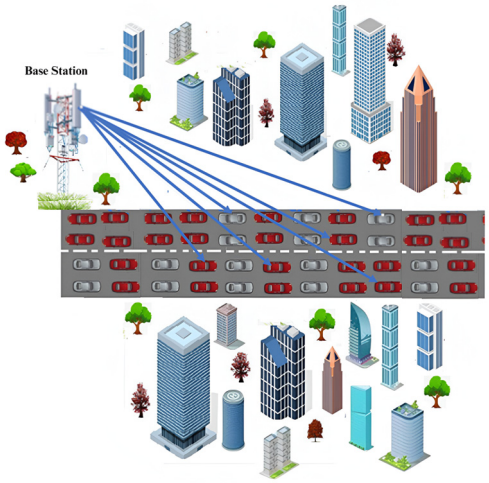

Fig. 3. Scenario of signal transmission at mmWave for the secure MIMO ZP-OTFS-SCMA system.

III. Block Diagram

In the previous section, we presented an overview of the OTFS-SCMA system. In this section, we highlight our proposed secure OTFS-SCMA system. A conceptual block diagram of the secure OTFS-SCMA system is shown in Fig. 4. Fig. 4 shows that six users are assumed to

receive their own transmitted data in the form of synthetically generated binary data. The binary data are encrypted using a 6-D hyperchaotic mapping system [7] and channel encoding using the Repeat and Accumulate (RA), Turbo, and LDPC channel coding techniques [21, 22]. The channel-encoded data are SCMA encoded and further processed to generate DS-gridded SCMA codes. The generated codes are used for delay-Doppler domain matrixed data generation and subsequently undergo inverse symplectic fast Fourier transformation; eventually, the Heisenberg transformation operation is executed on such preprocessed data prior to baseband equivalent signal transmission from the antenna port. At the receiving end of each user, the Minimum Mean Squared Error (MMSE) and Cholesky Decomposition-based Zero Forcing (CD-ZF) signal detection/channel equalization techniques are used [23, 24]. The detected signal undergoes Wigner transformation and is subsequently processed with a symplectic fast Fourier transformation scheme to regenerate DD gridded SCMA codes. Such codes are processed in SCMA decoding with an iterative factor graph-based Log-MPA multiuser detection algorithm, which has already been discussed in the previous section. However, the output of the SCMA decoding section contains channel-encoded binary data that are further processed for channel decoding and PLS decryption to recover the transmitted binary data of each of the six ground users.

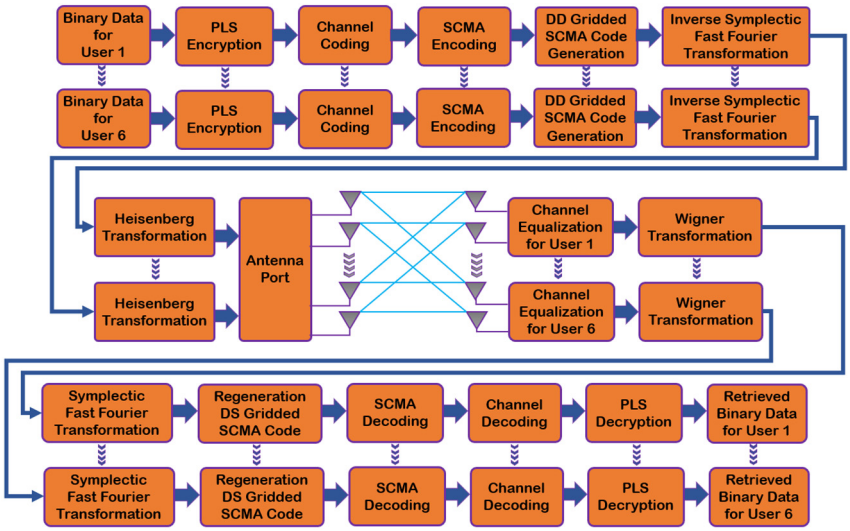

Fig. 4. Block diagram of the secure MIMO ZP-OTFS-SCMA system.

D. Signal Model

In this proposed system, the ground base station is considered to be composed of $N_T\ (=2)$ transmitting antennas, and each of the served six ground users riding in moving vehicles is equipped with $N_R\ (=2)$ receiving antennas. According to [7], the 6-D hyperchaotic mapping system can be written as:

$$\left\{\begin{array}{c}\dot{x}_1 = h(x_2 - x_1) + x_4 \\ \dot{x}_2 = -fx_2 - x_1x_3 + x_6 \\ \dot{x}_3 = -l + x_1x_2 \\ \dot{x}_4 = -x_2 - x_5 \\ \dot{x}_5 = kx_2 + x_4 \\ \dot{x}_6 = gx_1 + mx_2\end{array}\right\} \tag{9}$$

where $x_i (i = 1, 2, 3, 4, 5, 6)$ is the system variable and the system parameters $(h, f, l, k, g$ and $m)$ are assigned to $(20,\ 3.7,\ 200,\ 3,\ -5$ and $2)$ values. The initial values of the system variables are set to $(1.2,\ 1.3,\ 1.4,\ 1.5,\ 1.6,\ 1.7)$. The 8-bit integer-valued primary key K_0 of 14400×1 matrix in size can be generated and written as:

$$K_0 = \left\lceil \left| \frac{8.55}{6} \{x_1(t) + x_2(t) + x_3(t) + x_4(t) + x_5(t) + x_6(t)\} \right| \right\rceil \tag{10}$$

where $\lceil . \rceil$ indicates the rounding operation, and $(8.55/6)$ is a multiplication factor value used to confine K_0 values within the desirable range between 0 and 255. The primary key K_0 is disseminated into six encrypted keys $(K_1, K_2, \ldots\ldots, K_6)$, with each key containing 2400 elements and each element providing eight binary bits. The synthetically generated binary data b_k for the user, k is encrypted with its encrypted key, and we can write an encrypted binary data vector $\bar{b}_k$ of data length $\bar{N}$ as:

$$\bar{b}_k = b_k \oplus \bar{K}_k \tag{11}$$

where the symbol $\oplus$ indicates the XOR operation and $\bar{K}_k$ is the assigned key for user k in extended form. The encrypted binary data vector $\bar{b}_k$ is channel encoded to form a new binary data vector $\bar{\bar{b}}_k$ of data length $\bar{\bar{N}}$ depending on the coding rate of the channel coding technique used. In SCMA encoding, every two encoded bits of the individual user are mapped into $\bar{K}(=4)$-dimensional complex codebook to produce an SCMA-encoded data matrix $\tilde{X}$ of size $\bar{K} \times \bar{N}$, where $\bar{N}$ is the total number of symbols $\in \{0, 1, 2, 3\}$ of each user. In the data matrix $\tilde{X}$, $\bar{K}$ number of zeros are added at both ends of its column data, and a new data matrix $\ddot{X}$ of size $M \times \bar{N}$ is produced. The data matrix $\ddot{X}$ is reshaped to produce another delay-Doppler domain OTFS frame-based data

matrix $\ddot{X}$, and its matrix size is $M \times N \times L$, where M and N have already been specified in Fig. 1, and L is the number of OTFS frames. On execution of inverse symplectic fast Fourier transformation operation on delay-Doppler domain data matrix $\ddot{X}$, a time-frequency domain information sample matrix is generated and can be written as:

$$X_{tf}^{(l)}[j,k] = \frac{1}{\sqrt{NM}} \sum_{n=0}^{N-1} \sum_{m=0}^{M-1} \ddot{X}^{(l)}[m,n] e^{j2\pi\left(\frac{nk}{N} - \frac{mj}{M}\right)} \quad (12)$$

where, $l = 1,2,3 \ldots \ldots L, j = 0, \ldots, M-1$, $k = 0, \ldots, N-1$ and $X_{tf} \in \mathbb{C}^{(M \times N \times L)}$. In the Heisenberg transformation, frame-wise multiplication of X_{tf} signals with the diagonal matrix G_{tx} followed by row-wise vectorization are generated. G_{tx} can be written as:

$$G_{tx} = diag \left[g_{tx}(0), g_{tx}\left(\frac{T}{M}\right) \ldots \ldots g_{tx}\left(\frac{(M-1)T}{M}\right) \right] \in \mathbb{C}^{M \times N} \quad (13)$$

where T is the time duration of each OTFS frame and is equal to 1/carrier frequency spacing. However, in our case, we considered rectangular pulse-shaping waveforms and G_{tx} was reduced to I_M, where I_M is the $M \times M$ identity matrix. The Heisenberg-transformed signal $S_{tx}^{(l)}$ of matrix size $NM \times L$ can be written as:

$$S_{tx}^{(l)} = vec(G_{tx}.X_{tf}^{(l)}[j,k]) = vec\left(\frac{1}{\sqrt{NM}} \sum_{n=0}^{N-1} \sum_{m=0}^{M-1} \ddot{X}^{(l)}[m,n] e^{j2\pi\left(\frac{nk}{N} - \frac{mj}{M}\right)}\right) \quad (14)$$

where $l = 1,2,3 \ldots \ldots L, j = 0, \ldots, M-1, k = 0, \ldots, N-1$. Prior to transmission from the antenna port, the S_{tx} signal is disseminated into two independent frame-wise data streams and sent from each N_T transmitting antenna. The transmitted data signal $\vec{X} = \begin{bmatrix} \vec{X}_1 \\ \vec{X}_2 \end{bmatrix}$ is of $(2NM \times 0.5\,L)$ matrix in size. From the perspective of the peak-to-average power ratio (PAPR), the PAPR of the transmitted signal from each of the two transmitting channels can be written as:

$$PAPR_{ant=1,2} = \frac{max\left[\vec{X}_{ant=1.2}\right]^2}{E\left\{\left[\vec{X}_{ant=1.2}\right]^2\right\}} \quad (15)$$

where $E\{.\}$ and max denote the expected value and maximum value of the transmitted signal power, respectively. To evaluate the PAPR of the transmitted signal samples at each of the eight transmitting channels, the complementary cumulative distribution function (CCDF) is employed to measure the probability of the PAPR value exceeding a certain threshold value and can be written as:

$$P_r[PAPR(PAPR_{ant=1,2,\ldots\ldots 8} \geq PAPR_o = 1-(1-e^{-PAPR_o})^{\tilde{M}} \quad (16)$$

where $PAPR_o$ is the threshold value and $\tilde{M}$ is the total number of transmitted signal samples at each transmitting channel. In our study, we considered a four-path delay-Doppler domain channel model, and in such a model, the complex baseband channel impulse response for user k can be written as:

$$h_k^{ab}(\tau,\vartheta) = \sum_{i=1}^{i=4} g_{i,k}^{ab} e^{-j2\pi\vartheta_i\tau_i} \delta(\tau - \tau_i)\delta(\vartheta - \vartheta_i) \quad (17)$$

where $b = 1, N_T, a = 1, N_R$, $g_{i,k}^{ab}$ is the channel gain of the ith path considering the transmission link from the b^{th} base antenna to the a^{th} receiving antenna for user k, τ_i and ϑ_i are the delay and Doppler shift of the i^{th} path, respectively, and $\delta(\cdot)$ denotes the Dirac delta function. The complex baseband channel impulse response of Eq. (15) can be computed from the parameter values presented in Tables I and II.

As the discrete time equivalent channel vector h_k^{ab} has only four complex channel coefficients, it needs to be converted into an effective $NM \times NM$ circulant matrix for the multiplication of frame-wise NM samples from each of the N_T base station antennas. By adding $NM-4$ zeros with the h_k^{ab}, the new vector $\bar{h}_k^{ab}$ will be $1 \times NM$ matrix in size. The equivalent channel matrix H_k^{ab} can be written as:

$$H_k^{ab} = F_{NM}^*(diag\left(F_{NM}\left(\bar{h}_k^{ab}\right)^T\right))F_{NM} \quad (18)$$

where $F_{NM} = \frac{1}{\sqrt{NM}}\{e^{-j2\pi kl/NM}\}, k = 0,1,2, \ldots \ldots NM-1$, $l = 0,1,2, \ldots \ldots NM-1$ and F_{NM}^* are the inverse of the $NM-$point Discrete Fourier Transform (DFT) matrix, F_{NM} [16, 25].

From Eq. (16), the equivalent channel matrix for user 1 through user 6 can be written as:

$$H_1 = \begin{bmatrix} H_1^{11} H_1^{11} \\ H_1^{21} H_1^{22} \end{bmatrix}; H_2 = \begin{bmatrix} H_2^{11} H_2^{11} \\ H_2^{21} H_2^{22} \end{bmatrix};$$

$$H_3 = \begin{bmatrix} H_3^{11} H_3^{11} \\ H_3^{21} H_3^{22} \end{bmatrix}; \mathrm{H}_4 = \begin{bmatrix} \mathrm{H}_4^{11} \mathrm{H}_4^{11} \\ \mathrm{H}_4^{21} \mathrm{H}_4^{22} \end{bmatrix}; \quad (19)$$

$$\mathrm{H}_5 = \begin{bmatrix} \mathrm{H}_5^{11} \mathrm{H}_5^{11} \\ \mathrm{H}_5^{21} \mathrm{H}_5^{22} \end{bmatrix}; H_6 = \begin{bmatrix} H_6^{11} H_6^{11} \\ H_6^{21} H_6^{22} \end{bmatrix}$$

The size of the equivalent channel matrix assigned to each of the six users is $2NM \times 2NM$. The signal received by user k, Y_k, with a $2NM \times 0.5L$ matrix can be represented as:

$$Y_k = H_k \vec{X} + n_k \quad (20)$$

where $n_k \sim \mathbb{CN}(0_{2NM}.\sigma_n^2 I_{2NM})$ denotes the additive white Gaussian noise (AWGN). With the application of the Cholesky decomposition (CD)-based ZF signal detection technique addressed in [24], we need to multiply both sides of Eq. (20) by the term $(H_k^H H_k)^{-1} H_k^H$, and the received signal in a new form can be written as:

$$\bar{Y}_k = (H_k^H H_k)^{-1} H_k^H Y_k = (H_k^H H_k)^{-1} H_k^H H_k \vec{X} + (H_k^H H_k)^{-1} H_k^H n_k \quad (21)$$

On Cholesky decomposition of a matrix $(H_k^H H_k)$ into matrix $(L_k L_k^H)$, where L_k is the lower triangular matrix, Eq. (21) can be written as:

$$\tilde{Y}_k = (L_k L_k^H)^{-1} H_k^H H_k \vec{X} + (L_k L_k^H)^{-1} H_k^H n_k = \vec{X} + \vec{n}_k = \vec{\tilde{X}} \quad (22)$$

where $(L_k L_k^H)^{-1} H_k^H H_k$ is the $2NM \times 2NM$ identity matrix and $\vec{n}_k \sim \mathbb{CN}(0_{2NM}, \vec{\sigma}_n^2 I_{2NM})$ is the modified form of AWGN noise. Neglecting the noise term from Eq. (22), the detected signal $\vec{\tilde{X}}$ will be approximately equal to $\tilde{Y}_k$.

When the minimum mean square error (MMSE) signal detection technique is applied [23], the detected signal can be written as:

$$\vec{\hat{X}} = (H_k^H H_k + \sigma_n^2 I)^{-1} H_k^H Y_k \quad (23)$$

where σ_n^2 is the noise variance of the additive white Gaussian noise (AWGN).

The detected signal $\vec{\tilde{X}}/\vec{\hat{X}}$ is of $(2NM \times 0.5L)$ matrix in size, and it is reshaped to produce a data matrix $\bar{S}_{tx}^{(l)}$ of size $NM \times L$. It is converted to the delay-time matrix $\bar{Y}^{(l)} \in \mathbb{C}^{M \times N \times L}$ as:

$$\bar{Y}^{(l)} = G_{rx} \cdot \left(vec_{M,N}^{-1} \left(\bar{S}_{tx}^{(l)} \right) \right) \quad (24)$$

where G_{rx} is the receiver pulse shaping matrix and is identical to G_{tx}, the operator, $vec_{M,N}^{-1}$, which converts $\bar{S}_{tx}^{(l)} \in \mathbb{C}^{\mathrm{NM} \times \mathrm{L}}$ into $M \times N \times L$ sized matrix. In the Wigner transformation operation, the M-point DFT operation is performed on the delay-time matrix $\tilde{Y}^{(l)}$, and we can write the Wigner-transformed/time-frequency domain signal as:

$$Y_{tf}^{(l)} = F_M \bar{Y}^{(l)} \quad (25)$$

where M -point DFT, $F_M = \frac{1}{\sqrt{M}} \{ e^{-j2\pi m/M} \}$, $m = 0, 1, 2, \ldots \ldots M-1$.

By applying the Symplectic Fast Fourier transform (SFFT) to the time-frequency domain signal, $Y_{tf}^{(l)}$, we obtain the retrieved delay-Doppler domain OTFS frame-based data matrix $\ddot{Y}^{(l)}$ with size $M \times N \times L$, which can be written as:

$$\ddot{Y}^{(l)}[j,k] = \frac{1}{\sqrt{NM}} \sum_{n=0}^{N-1} \sum_{m=0}^{M-1} Y_{tf}^{(l)}[m,n] e^{-j2\pi \left(\frac{nk}{N} - \frac{mj}{M} \right)} \quad (26)$$

where $l = 1,2,3 \ldots \ldots L$, $j = 0, \ldots, M-1$, $k = 0, \ldots, N-1$. The data matrix $\ddot{Y}^{(l)}$ is reshaped into a new data matrix $\dddot{Y}$ of size $M \times \bar{N}$, and $\bar{K}$ number of zeros are removed from both ends of its column data to produce retrieved SCMA data matrix $\tilde{\tilde{X}}$ of size $\bar{K} \times \bar{N}$. In the application of the iterative factor graph-based Log-MPA detection algorithm, channel-encoded binary data for user k are retrieved. However, in our presented secure MIMO ZP-OTFS-SCMA system, its additional two parameters (throughput and latency) can be highlighted. In a very simplified form, we can estimate throughput in terms of channel capacity C_k for the user k. The channel capacity/ maximum data rate C_k [26] can be written using Shannon's theorem as:

$$C_k = [Blog_2(1 + \frac{\sigma_s^2}{\sigma_n^2})] \quad (27)$$

where σ_n^2 is the typically assumed noise power of -90 dBm, which corresponds to 1×10^{-12} watt of the AWGN noise added to the received signal at the user's receiver and σ_s^2 is the receive signal power, $B = M1\nabla f$, where $M1(= 12)$ is the number of delays (subcarrier) bins and $\nabla f (= 30\ kHz)$ is the subcarrier frequency spacing) is the system bandwidth,

$$C_{k-total} = \sum_{k=1}^{k=6} [Blog_2 (1 + \frac{\sigma_s^2}{\sigma_n^2})] \quad (28)$$

As in our system, we are using a channel encoder with consideration of its coding gain, R, the effective channel capacity or system throughput, which can be written as:

$$T_{system} = R \times C_{k-total} \quad (29)$$

In SCMA encoding, the sampling time, $T_s = \frac{1}{M1\nabla f} = 2.78 \times 10^{-6}$ second. In generating one SCMA codeword, it requires $4T_s$ second to accommodate two binary bits for each of the six users. The latency depends mainly on transmission time, processing Delay, propagation delay, and protocol overhead [26].

E. Complexity Analysis

In our system, we utilized the Log-MPA algorithm for SCMA decoding at the receiving end of each user. At the transmitting end, each resource element is shared by three $(df = 3)$ users. In terms of df, K (= 4, no. of resource elements), N_{iter} (no. of message passing iterations), $\widehat{M}$(= 4, no. of codewords in the SCMA codebook) and $\widehat{N}$(= 2, degree of the variable nodes, VNs), the computational decoding complexity with the Log-MPA algorithm requires $\{3\widehat{M}^{d_f} K d_f^2 N_{iter} + 2\widehat{M} K d_f + 3\widehat{M}^{d_f} K d_f N_{iter} + 4\widehat{M} K d_f + \widehat{M}^{d_f} K d_f N_{iter} + (\widehat{N} - 2)\widehat{M}^{d_f} K d_f N_{iter}\}$ operations [27]. In the case of MMSE signal detection, the size of the effective MIMO channel matrix for each of the six users is $2NM \times 2NM$, and in such linear signal detection, inversion of $2MN \times 2MN$ matrices will be necessary, and computational detection complexity requires $(2MN)^3$ operations [28]. In CD-based ZF signal detection, computational detection complexity requires $2NM\ (2NM + 1)\ (2NM + 2)/6$ operations [24].

BER Calculation Algorithm 1 for Individual Users as follow:

Algorithm 1 BER Calculation Algorithm for Individual User

1. Input: Binary data, information provided in Table II
2. Initialization: BER values are zero for user $\boldsymbol{k}$, $\boldsymbol{BER_k = 0}$
3. for user $\boldsymbol{k} \in [\boldsymbol{1}, \boldsymbol{K}]$ do
4. Encrypt binary data $\bar{\boldsymbol{b}}_{\boldsymbol{k}} = \boldsymbol{b_k} \oplus \bar{\boldsymbol{K}}_{\boldsymbol{k}}$ using Eq. (11)
5. Execute channel coding and generate SCMA-encoded data using Eq. (1)
6. Generate DS gridded SCMA code
7. Execute inverse symplectic fast Fourier transformation operation Eq. (12)
8. Execute the Heisenberg transformation operation using Eqn. (13) and (14)
9. Generate transmitted data signal $\vec{\boldsymbol{X}}$ from the signal model presented in Eq. (14)
10. Generate receive signal $\boldsymbol{Y_k}$ for the user k using Eq. (20)
11. Detect the user's own transmitted signal $\bar{\bar{\boldsymbol{X}}}$ using CD-ZF-based signal detection scheme using Equation (22)
12. Detect the user's own transmitted signal $\hat{\hat{\boldsymbol{X}}}$ using MMSE signal detection scheme using Eq. (23)
13. Execute the Wigner transformation operation using Eqn. (24) and (25)
14. Execute Symplectic Fast Fourier Transform (SFFT) operation using Eq. (26)
15. Extract SCMA encoded data from the signal model of Eq. (26)
16. Implement Log-MPA detection algorithm on extracted SCMA encoded data, $\tilde{\tilde{\boldsymbol{X}}}$
17. Execute channel decoding
18. Execute PLS decryption and decrypt binary data $\tilde{\boldsymbol{b}}_{\boldsymbol{k}}$
19. $\boldsymbol{BER_k = BER_k + sum(not(\tilde{b}_k == b_k))}$;
20. End for
21. Output: $\boldsymbol{BER_k}$;

III. Simulation and Numerical Results

In this section, numerical results are presented and analyzed for a secure MIMO ZP-OTFS-SCMA system. In Table I, various useful information on the excess tap delay and relative power assigned to different users is provided, which would be helpful for computing time-varying effective fading channels. Other simulation parameters are presented in Table II. Fig. 5 and Fig. 6 present bifurcation diagrams of commensurate six-dimensional (6-D) hyperchaotic systems in the 3-D phase and generated keys assigned to different users for PLS encryption.

Due to PLS encryption, the encrypted binary data becomes confidential, and without knowing the encryption keys, obtaining the original transmitted binary data is impossible. In the comparison of the original binary data with the encrypted for User 1, User 2, User 3, User 4, User 5 and User 6, the correlation coefficients are found to have values of 15.54%, 16.00%, 26.11%, 22.39%, 19.45% and 18.68%, respectively.

Upon thorough examination of the graphical representations shown in Figs. 7 through 12, it is quite obvious that the presently considered secure OTFS-SCMA system shows the worst performance in the case of implementing LDPC channel coding with the CD-based Zero-Forcing (ZF) signal detection technique and robust BER performance under the scenario of implementing Turbo channel coding with the CD-based zero-forcing (ZF) signal detection technique.

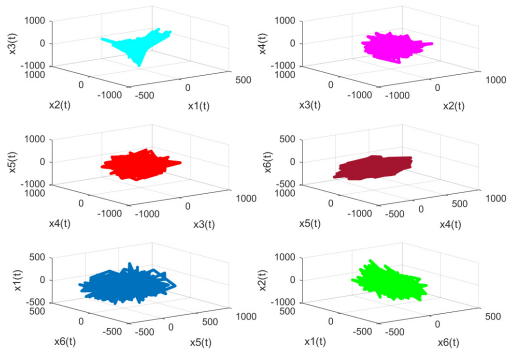

Fig. 5. Bifurcation diagrams of commensurate six-dimensional (6-D) hyperchaotic system in 3-D phase.

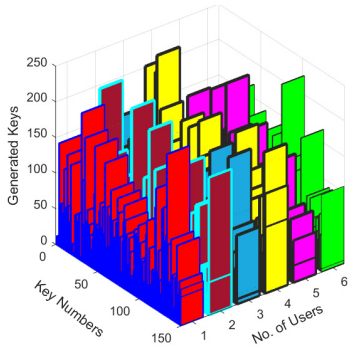

Fig. 6. Keys for different users generated using a six-dimensional (6-D) hyperchaotic system.

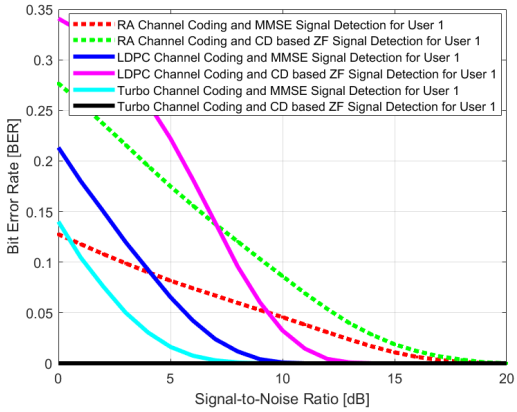

Fig. 7. BER performance of the considered OTFS-SCMA system utilizing various channel coding and signal detection techniques for User 1.

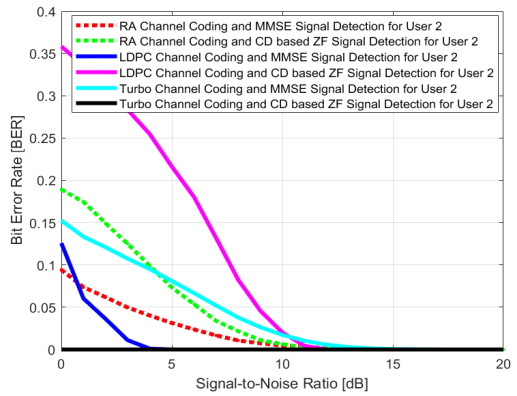

Fig. 8. BER performance of the considered OTFS-SCMA system utilizing various channel coding and signal detection techniques for User 2.

TABLE I. EXCESS TAP DELAY (μs) AND RELATIVE POWER (dB) ASSIGNED TO DIFFERENT USERS

User	Excess tab delay (μs)				Relative power (dB)			
User 1	0	5	10	15	0	−3	−6	−9
User 2	0	6	12	18	0	−4	−7	−10
User 3	0	7	14	21	0	−5	−8	−11
User 4	0	8	16	24	0	−6	−9	−12
User 5	0	9	18	27	0	9	18	27
User 6	0	10	20	30	0	−8	−11	−14

TABLE II. SIMULATION PARAMETERS

Description	Value
No. of users	6
Input data type and its number	Binary, 1200
mmWave carrier frequency (GHz)	28
Subcarrier spacing (KHz)	30
No. of OTFS frame	100
UE speed (km/h)	30, 60, 90, 120, 150, 180
Time duration of a single OTFS frame (micro sec)	33.33
Sampling time (micro-sec)	2.78
Size of a OTFS frame (M, N)	(12,12)
Total signal bandwidth (KHz)	360
Antenna configuration	{2,2,2,2,2,2} ×2
Channel Coding Technique	Repeat and Accumulated (RA), LDPC and Turbo
Signal Detection/Channel Equalization Technique	MMSE and Cholesky Decomposition based ZF (CD-ZF)
SCMA decoding algorithm	Iterative factor graph-based Log-MPA
Signal-to-noise ratio (dB)	0-20

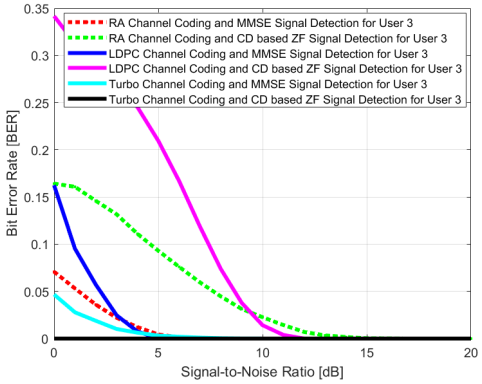

Fig. 9. BER performance of the considered OTFS-SCMA system utilizing various channel coding and signal detection techniques for User 3.

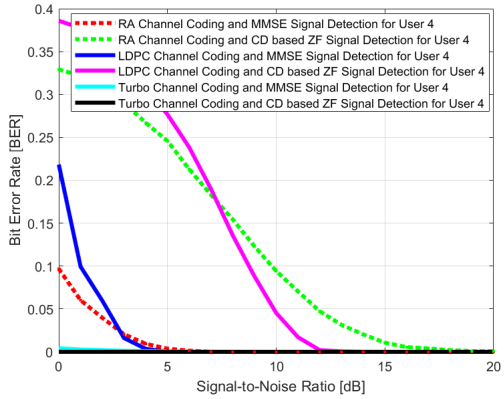

Fig. 10. BER performance of the considered OTFS-SCMA system utilizing various channel coding and signal detection techniques for User 4.

It can be seen from the graphical illustration presented in Fig. 7 with consideration of a typically assumed SNR of 5 dB that the estimated BERs for User 1 are 0%, 0.03%, 7.58%, 16.67%, 5.83%, and 24% under the utilization of Turbo with CD-ZF, Turbo with MMSE, RA with MMSE, and RA with CD-ZF, LDPC with MMSE and LDPC with CD-ZF viz, respectively. The BER value ranges from 0% to 24%. At the typically assumed 10% BER, SNR gains of 1 dB, 3.3 dB, 6.7 dB, and 8 dB are achieved in Turbo with MMSE compared to RA with MMSE, LDPC with MMSE, LDPC with CD-ZF and RA with CD-ZF. In the case of all other users (Users 2 to 6) and their simulated BER results (Figs. 8 through 12), analysis will be performed for identical 10% BER and BER values at 5 dB SNR under identical utilization of Turbo with CD-ZF, Turbo with MMSE, RA with MMSE and RA with CD-ZF, LDPC with MMSE and LDPC with CD-ZF as user 1. From Fig. 8 for User 2, it is noticeable that the SNR gains of 2.55 dB, 3.55 dB, and 7.05 dB are achieved in the LDPC with the MMSE compared to the Turbo with the MMSE, the RA with the CD-ZF and the LDPC with the CD-ZF, respectively. The estimated BERs are found to be 0%, 8.5%, 3.3%, 6.75%, 0%, and 24.67%, viz. The BER varies from 0% to 24.67%. For User 3 from Fig. 10, the estimated BERs are 0%, 0.33%, 0.08%, 9.25%, 0% and 22.42%, viz. The BER varies from 0% to 24.42%. In the case of SNR gain, LDPC with MMSE achieves SNR gains of 3.90 dB and 8.30 dB compared to RA with CD-ZF and LDPC with CD-ZF. From Fig. 10 for User 4, we obtained SNR gains of 6.60 dB and 8.00 dB for the utilization of LDPC with MMSE as compared to LDPC with CD-ZF and RA with CD-ZF, and the estimated BER values (0%, 0.05%, 0.08%, 23.33%, 0% and 27.75%) varied from 0% to 27.75%. Fig. 11 shows that the estimated BERs for User 5 are 0%, 0.53%, 3.33%, 13.92%, 1.67%, and 21.08%, which indicate BERs ranging from 0% to 21.08%. In the case of SNR gain, RA with MMSE achieves SNR gains of 3.30 dB, 4.50 dB, and 5.50 dB compared to LDPC with MMSE, RA with CD-ZF, and LDPC with CD-ZF, respectively. Fig. 12 for User 6 shows that the estimated BERs are 0%, 3.20%, 1.30%, 18.17%, 0, and 21.67%, viz. The BER ranges from 0% to 21.67%. Figure 12 also shows that we are getting SNR gains of 1.30 dB, 7.80 dB, and 8.50 dB in RA with MMSE as compared to LDPC with MMSE, LDPC with CD-ZF, and RA with CD-ZF, respectively. In our study, we investigate an OTFS-SCMA system model with a Base Station (BS) equipped with six transmitting antennas and six downlink users. Each user is equipped with two receiving antennas. We consider two cases, and in one case, we assign six users that correspond to vehicular velocities of 30 km/h, 60 km/h, 90 km/h, 120 km/h, 150 km/h, and 180 km/h and the maximum. The Doppler shifts are 778.32

Hz, 1.56 kHz, 2.33 kHz, 3.11 kHz, 3.89 kHz, and 4.67 kHz, respectively. In addition, the vehicular velocities are 20 km/h, 40 km/h, 60 km/h, 80 km/h, 100 km/h, and 120 km/h, and the estimated maximum Doppler shifts are 518.88 Hz, 1.04 kHz, 1.56 kHz, 2.08 kHz, 2.59 kHz, and 3.11 kHz, respectively. These estimated maximum Doppler shift values are much less than our chosen subcarrier spacing (30 kHz), which can effectively reduce the Interchannel Interference (ICI) introduced by the time-varying channels.

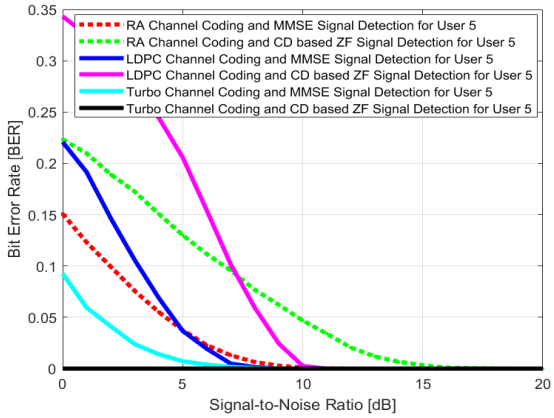

Fig. 11. BER performance of the considered OTFS-SCMA system utilizing various channel coding and signal detection techniques for User 5.

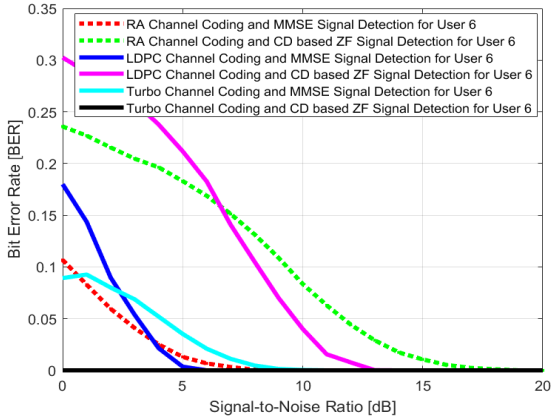

Fig. 12. BER performance of the considered OTFS-SCMA system utilizing various channel coding and signal detection techniques for User 6.

For our system, we have estimated channel capacity for each of the six ground users. The estimated channel capacity for Users 1, 2, 3, 4, 5, and 6 are found to have values of 13.41 Mbps, 13.28 Mbps, 12.97 Mbps, 13.11 Mbps, 13.22 Mbps, and 12.87 Mbps with a total channel capacity of the system is of 78.84 Mbps. Assuming a channel coding gain of $\frac{1}{2}$ in the case of RA and LDPC and 0.3322 in the case of turbo coding, the system throughput underutilization of turbo channel coding is 26.1906 Mbps. In the case of RA/LDPC channel coding, the estimated system throughput would be 39.4200 Mbps. In addition to estimating system throughput, we have also estimated latency. In our system, we consider that the number of bits to be transmitted for each of the six users is 2400. For 2-bit transmission, it requires $4T_s$ second, in such a case, the data rate would be 180 kbps. In estimating latency, transmission time can be calculated as:

$$Transmission\ Time = \frac{2400}{180000} = 0.0133\ s = 13.3\ ms \quad (30)$$

We consider that for both processing delay and protocol overhead, the time required is 10 msec. Let's further consider that the distance of the six users from the ground base station is identical, with a typically assumed distance of 200 m. In such a case, T is the propagation delay time, which is 66.67 μs, and the total latency for data transmission for each user $= 13.3 + 10 + 0.066 + 10 = 33.37\ ms$.

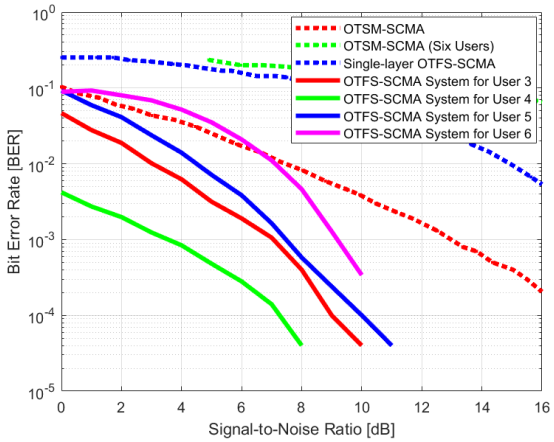

Fig. 13. Bit Error Rate (BER) against the Signal-to-Noise Ratio (SNR) for the proposed OTFS-SCMA system with other OTFS-SCMA and its variant systems.

Fig. 13 compares the Bit Error Rate (BER) against the Signal-to-Noise Ratio (SNR) between the proposed OTFS-SCMA system and other OTFS-SCMA varied systems. In our OTFS-SCMA system, BER performance with the utilization of the Turbo channel coding and MMSE signal detection techniques has been shown for Users 3, 4, 5, and 6. In the case of User 1 and User 2, BERs are found to have zero values, which have not been shown in Fig. 13. Thomas *et al.* [11] performed a comprehensive study on a downlink system that combines Orthogonal-Time-Frequency-Space (OTFS) modulation and sparse code multiple access (SCMA) to support massive connectivity in high-mobility environments. In their study, the BER performance of the OTSM-OMA system was compared with that of the OTSM-SCMA system under consideration of an identical number (= 32) of subcarriers and time slots, 15 kHz carrier frequency shift with 4 GHz carrier frequency and 5 propagation paths present in the channel. Deka *et al.* [29] designed a framework for an OTFS-SCMA system. In their BER performance study, the total number of sub-carriers and time slots was 8, and their OTFS-SCMA system involved 6 users with an overloading factor of 150%. Wen *et al.* [30] developed a novel downlink code-domain NOMA scheme by integrating OTFS and SCMA and proposed a single-layer cross-domain detection algorithm for OTFS SCMA

systems. In very few cross-domain iterations, significant BER performance gains were achieved. In Fig. 13, the BER performance results against the normalized SNRs (E_b/N_0) have been converted into SNRs.

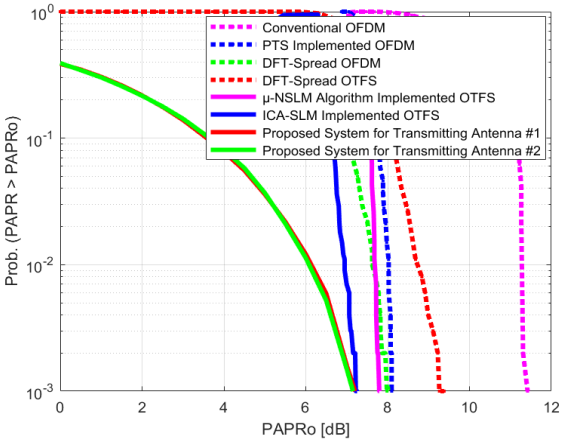

Fig. 14. Comparison of the CCDFs of the PAPR of the considered OTFS-SCMA system with the other PAPR reduction algorithms implemented and DFT-Spread (OTFS and OFDM) systems.

From a PAPR standpoint, it is evident that the signals transmitted from the first and second transmitting antennas have estimated PAPRs of 6.55 dB and 6.67 dB, respectively, confirming an average value of 6.61 dB. Fig. 14 shows the Complementary Cumulative Distribution Functions (CCDFs) of the PAPR of our system and the PAPR reduction schemes (μ-normalized selective mapping, imperialist competition algorithm-aided selective mapping, DSP spreading) implemented in the OTFS and OFDM systems [31–34]. It is quite obvious from Fig. 14 that our proposed OTFS-SCMA system, without the utilization of any PAPR reduction scheme, shows comparatively enhanced PAPR reduction performance. For a typically assumed 1×10^{-3} CCDF of PAPR value (greater than the threshold), the estimated values of PAPR in the case of our system, ICA-SLM-implemented OTFS, μ-NSLM-implemented OTFS, DFT spread OFDM, PTS implemented OFDM, DFT-Spread OTFS and conventional OFDM system are 6.61 dB, 7.25 dB, 7.80 dB, 7.98 dB, 8.10 dB, 9.26 dB and 11.40 dB, respectively. From such presented PAPRs, we can demonstrate that the PAPR for the transmitting signal of our system decreases by 4.79 dB, 2.65 dB, 1.49 dB, 1.37 dB, and 0.64 dB in contrast with the transmitting signal of conventional OFDM, DFT spread OTFS, PTS implemented OFDM, DFT spread OFDM and μ-NSLM implemented OTFS systems, respectively. Compared with the ICA-SLM-implemented OTFS system, our system achieves comparable PAPR performance. In a nutshell, we have proposed a secure future generation spectrally efficient wireless communication system. BER analysis is one of the essential performance metrics of a typically assumed wireless communication system. The estimated BER performance results, along with the proper selection of Turbo channel coding and CD-ZF signal detection techniques in our proposed system, can provide direction to future research activity in both industry and academia.

In this study, we also compare numerically estimated results with the previous works presented in tabular form (Table III). Table III presents BER performance results underutilization of Turbo channel coding and MMSE signal detection techniques. The results presented in Table II confirm that our proposed system's PAPR and BER performance are comparatively better than those of other systems.

TABLE III. COMPARISON OF SIMULATION RESULTS WITH PREVIOUS WORKS

System type	PAPR (dB) at CCDF of PAPR (1×10^{-3})	Estimated Bit Error Rate (BER) at 5 dB SNR	References
OTSM-SCMA		0.02131	[11]
OTFS-NOMA based on SCMA (six users)		0.2327	[29]
Single layer OTFS-SCMA		0.1723	[30]
μ- NSLM algorithm implemented OTFS system	7.80	0.3291	[32]
DFT-s-OTFS system	9.26	0.06127	[33]
DFT-s-OFDM system	7.98		[35]
Proposed system	6.61	0.0003–0.0323	

IV. CONCLUSIONS

In this paper, we have presented a framework for a designed transceiver of Orthogonal Time Frequency Space (OTFS) system integrated with Sparse code multiple access (SCMA) system to support multiuser narrow band data transmission in high-mobility environments. Our proposed system has been formed by integrating two different schemes (OTFS and SCMA), and we can undoubtedly exploit their advantages. The simulation outcome proves the effectiveness of the proposed system with improved BER performance compared to other OTFS-SCMA systems and their variants. From the perspective of the PAPR, our proposed system presents a reasonably acceptable PAPR compared to the other PAPR reduction algorithms implemented and DFT-Spread (OTFS and OFDM) systems. Based on the estimated BERs and PAPRs, it may be concluded that the proposed secure MIMO ZP-OTFS-SCMA system is very robust and effective in multiuser data transmission under the utilization of Turbo channel coding and the Cholesky Decomposition-based ZF (CD-ZF) signal detection technique.

In this study, we obtained robust BER performance and reasonably acceptable PAPR performance without the applicability of any PAPR reduction techniques/algorithms. In addition to the PAPR and BER performance study, we need to focus on presenting an analytical expression of estimating SINR based on which we can estimate the user's achievable ergodic spectral

efficiency and system spectral efficiency. To the best of our knowledge, such challenging tasks have not yet been appropriately addressed in our proposed multiuser secure OTFS- SCMA system and other variants of OTFS- SCMA system, and it can be an interesting research topic for the future.

CONFLICT OF INTEREST

The author declares no conflict of interest.

AUTHOR CONTRIBUTIONS

Md. Najmul Hossain is responsible for the overall research project's conceptualization, planning, and execution, including research supervision, writing original draft reviews, editing, and funding acquisition. SK. Tamanna Kamal and Jinia Rahman participated in data analysis and interpretation of simulation results, and they implemented coding and simulation tools necessary for performance evaluation using MATLAB software. Shaikh Enayet Ullah provided expertise in specific technical aspects related to physical layer security. Lastly, Tetsuya Shimamura provided input on practical implications and potential applications of the research and review the manuscript; all authors had approved the final version.

ACKNOWLEDGMENT

The authors sincerely thank Saitama University and Prof. Tetsuya Shimamura for their support and research resources.

REFERENCES

[1] P. Yang, Y. Xiao, M. Xiao, and S. Li, "6G wireless communications: vision and potential techniques," *IEEE Network*, vol. 33, no. 4, pp. 70–75, July/August 2019. doi: 10.1109/MNET.2019.1800418

[2] Wei *et al*., "Orthogonal time-frequency space modulation: A promising next-generation waveform," *IEEE Wireless Communications*, vol. 28, no. 4, pp. 136–144, August 2021. doi: 10.1109/MWC.001.2000408

[3] W. Yuan *et al*., "New delay Doppler communication paradigm in 6G era: A survey of Orthogonal Time Frequency Space (OTFS)," *China Communications*, vol. 20, no. 6, pp. 1–25, June 2023. doi: 10.23919/JCC.fa.2022-0578.202306

[4] H. Tataria, M. Shafi, A. F. Molisch, M. Dohler, H. Sjöland, and F. Tufvesson, "6G wireless systems: Vision, requirements, challenges, insights, and opportunities," in *Proc. the IEEE*, July 2021, vol. 109, no. 7, pp. 1166–1199. doi: 10.1109/JPROC.2021.3061701

[5] L. Miuccio, D. Panno, and S. Riolo, "A flexible encoding/decoding procedure for 6g SCMA wireless networks via adversarial machine learning techniques," *IEEE Transactions on Vehicular Technology*, vol. 72, no. 3, pp. 3288–3303, March 2023. doi: 10.1109/TVT.2022.3216028

[6] P. Liu, J. Lei, and W. Liu, "Learning-based latency and energy optimization in SCMA-enhanced UAV-MEC networks," in *Proc. 2023 IEEE/CIC International Conference on Communications in China (ICCC)*, Dalian, China, 2023, pp. 1–6. doi: 10.1109/ICCC57788.2023.10233490

[7] S. Sun, "A new image encryption scheme based on 6D hyperchaotic system and random signal insertion," *IEEE Access*, vol. 11, pp. 66009–66016, 2023. doi: 10.1109/ACCESS.2023.3290915

[8] Y. Ge, Q. Deng, D. G. G., Y. L. Guan and Z. Ding, "OTFS signaling for SCMA with coordinated multi-point vehicle communications," *IEEE Transactions on Vehicular Technology*, vol. 72, no. 7, pp. 9044–9057, July 2023. doi: 10.1109/TVT.2023.3248119

[9] L. Bai *et al*., "Performance analysis of multicarrier modulation waveforms for terahertz wireless communication," in *Proc. 2023 21st International Conference on Optical Communications and Networks (ICOCN)*, Qufu, China, 2023, pp. 1–3. doi: 10.1109/ICOCN59242.2023.10236228

[10] K. Deka, A. Thomas, and S. Sharma, "OTFS-SCMA: A code-domain NOMA approach for orthogonal time frequency space modulation," *IEEE Transactions on Communications*, vol. 69, no. 8, pp. 5043–5058, Aug. 2021. doi: 10.1109/TCOMM.2021.3075237

[11] A. Thomas, N. Sangeeta, K. Deka, S. Sharma, and A. Rajesh, "OTSM-SCMA: Code-domain NOMA based orthogonal time sequency multiplexing modulation," in *Proc. 2023 National Conference on Communications (NCC)*, Guwahati, India, 2023, pp. 1–6. doi: 10.1109/NCC56989.2023.10067992

[12] Q. Deng, Y. Ge, and Z. Ding, "Jamming suppression via resource hopping in high-mobility OTFS-SCMA systems," *IEEE Wireless Communications Letters*, vol. 12, no. 12, pp. 2138–2142, Dec. 2023. doi: 10.1109/LWC.2023.3309787

[13] Y. Ge, L. Liu, S. Huang, D. G. G., Y. L. Guan, and Z. Ding, "Low-complexity memory AMP detector for high-mobility MIMO-OTFS SCMA systems," in *Proc. 2023 IEEE International Conference on Communications Workshops (ICC Workshops)*, Rome, Italy, 2023, pp. 807–812. doi: 10.1109/ICCWorkshops57953.2023.10283752

[14] J. Li and Y. Hong, "Performance analysis and phase shift design of IRS-aided uplink OTFS-SCMA," *IEEE Access*, vol. 11, pp. 133059–133069, 2023, doi: 10.1109/ACCESS.2023.3336677

[15] Y. Zhang *et al*., "Constant modulus codebook design for SCMA system," in *Proc. 2018 IEEE International Conference on Communication Systems (ICCS)*, Chengdu, China, 2018, pp. 242–246. doi: 10.1109/ICCS.2018.8689235

[16] Y. Hong, T. Thaj, and E. Viterbo, *Delay-Doppler Communications: Principles and Applications*, 1st ed., Elsevier, USA, February 2022.

[17] D. G. Harkut and K. N. Kasat**,** "Coding theory essentials," *IntechOpen*, 2023.

[18] M. Taherzadeh, H. Nikopour, A. Bayesteh, and H. Baligh, "SCMA codebook design," in *Proc. 2014 IEEE 80th Vehicular Technology Conference (VTC2014-Fall)*, IEEE, 2014, pp. 1–5. doi: 10.1109/VTCFall.2014.6965882

[19] K. Han, J. Hu, J. Chen, and G. E. Sobelman, "A low complexity SCMA detector based on stochastic computation," in *Proc. 2017 IEEE 60th International Midwest Symposium on Circuits and Systems (MWSCAS)*, IEEE, 2017, pp. 783–786. doi: 10.1109/MWSCAS.2017.8053098

[20] S. Jaber, W. Chen, and K. Wang, "SCMA spectral and energy efficiency with QoS," *IEEE Access*, vol. 9, pp. 37410–37417, 2021. doi: 10.1109/ACCESS.2021.3062025

[21] G. A. Vitetta, D. P. Taylor, G. Colavolpe, F. Pancaldi, and P. A. Martin, *Wireless Communications: Algorithmic Techniques*, John Wiley & Sons, March 29, 2013.

[22] Y. Jiang, *A Practical Guide to Error-Control Coding Using MATLAB*, Artech House, 2010.

[23] Y. S. Cho, J. Kim, W. Y. Yang, and C. G. Kang, *MIMO-OFDM Wireless Communications with MATLAB*, John Wiley & Sons, 2010.

[24] R. Gangarajaiah, H. Prabhu, O. Edfors, and L. Liu, "A Cholesky decomposition based massive MIMO uplink detector with adaptive interpolation," in *Proc. 2017 IEEE International Symposium on Circuits and Systems (ISCAS)*, IEEE, 2017, pp. 1–4.

[25] Y. A. Al-Jawhar, K. N. Ramli, M. A. Taher, N. S. M. Shah, L. Audah, and M. S. Ahmed, "Zero-padding techniques in OFDM systems," *International Journal on Electrical Engineering and Informatics*, vol. 10, no. 4, pp. 704–725, 2018.

[26] V. Garg, *Wireless Communications & Networking*, Elsevier, 2010.

[27] J. Liu, G. Wu, S. Li, and O. Tirkkonen, "On fixed-point implementation of Log-MPA for SCMA signals," *IEEE Wireless Communications Letters*, vol. 5, no. 3, pp. 324–327, 2016. doi: 10.1109/LWC.2016.2533051

[28] M. H. Abid, I. A. Talin, and M. I. Kadir, "Reconfigurable intelligent surface-aided orthogonal time frequency space and its deep learning-based signal detection," *IEEE Access*, 2023.

[29] K. Deka, A. Thomas, and S. Sharma, "OTFS-NOMA based on SCMA," arXiv preprint, arXiv:2005.03216, 2020.

[30] H. Wen, W. Yuan, Z. Liu, and S. Li, "OTFS-SCMA: A downlink NOMA scheme for massive connectivity in high mobility channels," *IEEE Transactions on Wireless Communications*, 2023.

[31] X. Xu, P. Yang, B. Zhang, Y. Xiao, and S. Li, "An improved PAPR reduction method based on imperialist competition algorithm for OTFS system," in *Proc. 2022 IEEE 96th Vehicular Technology*

Conference (VTC2022-Fall), IEEE, 2022, pp. 1–6. doi: 10.1109/VTC2022-Fall56434.2022.10001234

[32] J. Bai, B. Lin, and X. Tao, "Improved PAPR reduction algorithm for OTFS systems," in *Proc. 2023 19th International Conference on Natural Computation, Fuzzy Systems and Knowledge Discovery (ICNC-FSKD)*, IEEE, 2023, pp. 1–6. doi: 10.1109/ICNC-FSKD57052.2023.10023456

[33] Y. Wu, C. Han, and Z. Chen, "DFT-spread orthogonal time frequency space system with superimposed pilots for terahertz integrated sensing and communication," *IEEE Transactions on Wireless Communications*, vol. 22, no. 11, pp. 7361–7376, 2023. doi: 10.1109/TWC.2023.3000123

[34] Y. A. Al-Jawhar, K. N. Ramli, M. A. Taher, N. S. Mohd Shah, S. A. Mostafa, and B. A. Khalaf, "Improving PAPR performance of filtered OFDM for 5G communications using PTS," *ETRI Journal*, vol. 43, no. 2, pp. 209–220, 2021. doi: 10.4218/etrij.2021-0086

[35] H. G. Myung, J. Lim, and D. J. Goodman, "Single carrier FDMA for uplink wireless transmission," *IEEE Vehicular Technology Magazine*, vol. 1, no. 3, pp. 30–38, 2006. doi: 10.1109/MVTM.2006.1649597